A Truly Redundant Aerial Manipulator System with Application to Push-and-Slide Inspection in Industrial Plants

Marco Tognon, Hermes A Tello Chávez, Enrico Gasparin, Quentin Sablé, Davide Bicego, Anthony Mallet, Marc Lany, Gilles Santi, Bernard Revaz, Juan Cortés, et al.

A Truly Redundant Aerial Manipulator System with Application to Push-and-Slide Inspection in Industrial Plants

Marco Tognon[1], Hermes A. Tello Chávez[1], Enrico Gasparin[2], Quentin Sablé[1], Davide Bicego[1], Anthony Mallet[1], Marc Lany[2], Gilles Santi[2], Bernard Revaz[2], Juan Cortés[1], Antonio Franchi[1]

***Abstract*— We present the design, control and motion planning of an aerial manipulator for a non-trivial physical interaction task, namely pushing while sliding on curved surfaces. The proposed robotic system is motivated by the increasing interest on autonomous Non-Destructive Tests used for the integrity assessment of industrial plants. The proposed aerial manipulator consists of a multidirectional-thrust aerial vehicle to enhance physical interaction capabilities, endowed with a 2-DoFs lightweight arm to enlarge its workspace. This combination constitutes a truly redundant manipulator that goes beyond standard aerial manipulators with collinear multirotors. The robot controller is based on a PID method with 'displaced' positional part inspired by controllers for manipulators with elastic joints and grounded on several experimental trial-and-error tests. In this work we experimentally show that the proposed aerial manipulator system, equipped with an Eddy Current probe, is able to scan a metallic pipe sliding the sensor over its surface and preserving the contact. From the acquired data, a weld on the pipe is successfully detected and mapped.**

I. INTRODUCTION

In industrial facilities, the assessment of the structural integrity is a mandatory process to be performed regularly. For example, the periodic control of pipeline networks constitutes a common task in sectors like oil&gas and water industries. In those and many other sectors, Non-Destructive Testing (NDT) or Evaluation (NDE) plays a very important role. They allow to assess the status of an industrial plant without damaging its parts or altering its properties. Among all the various tests required in an oil&gas-like plant, the integrity inspection of low carbon steel welds over pipes is very frequent. They might have cracks or defects.

Among the available NDT techniques for weld inspection, the *Eddy-Current* (EC) [1] is particularly advantageous because does not require the preparation of the inspecting surface. Furthermore, the EC method is also used for other applications, like the wall-thinning of insulated pipes.

Nowadays, the inspection task is typically conducted by human operators that often have to access dangerous areas (e.g., elevated points) with the use of hazardous equipment like climbing ropes or temporary scaffolds. This aspect led to a growing interest in the development and deployment of structural health monitoring solutions [2] or remotely operated inspections by means of robots. The enhancement introduced by an automated system is not only limited to safety. It allows to generate very useful inspections maps [3] as well. In fact, the precise location of a weld on a pipe is not always known a priori, and is neither easily retrievable with visual sensors. Besides, pipes are very often painted or covered by insulating materials.

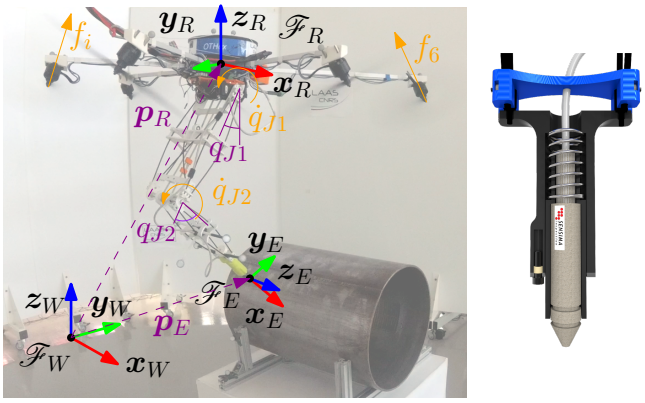

Fig. 1: Aerial manipulator with main variables on the left. On the right a sliced visualization of the compliant sensor holder.

However, the inspection task is challenging for a robot since it involves accurate physical interaction. In particular, the probe have to be always in contact with the surface during its scan. This contact-based inspection is only one example of the many other applications requiring robots to slide an end-effector on a curved surface while pushing it against the surface, ensuring the contact. Both pose of the end-effector and interaction force have to be accurately controlled.

At present, underwater EC inspections are a concrete reality. Submarines ROV are equipped with manipulators to perform such inspections of oil rigs and offshore platforms[1]. Driven by the industrial sector, the extension to aerial inspection is also gaining a lot of interest in the last years. However, aerial vehicles are still practically employed only for passive tasks as inspection and surveillance using sensors like cameras. This because the challenging nature of aerial physical interaction that is currently under investigation by several research labs and European projects like *Aeroarms* [4].

In the recent research literature, we can find several aerial system and methods proposed to face the aerial physical

[1]LAAS-CNRS, Université de Toulouse, CNRS, Toulouse, France, mail@laas.fr, antonio.franchi@laas.fr,
[2]SENSIMA INSPECTION, Av. Mont Blanc 31, 1196 Gland, Switzerland www.sensimainsp.com, info@sensimainsp.com

This work has been funded by the European Union's Horizon 2020 research and innovation programme under grant agreement No 644271 AEROARMS.

This paper is also the result of the preliminary work done by Markus Ryll.

[1]Sensima Inspection: Electro-Magnetic Solutions for Industrial Inspection, http://www.sensimainsp.com

interaction problem. They range from unidirectional-thrust aerial vehicles (like quadrotors) endowed with rigid [5] or articulated arms [6], to more recent multidirectional-thrust vehicles characterized by a superior interaction capability [7]. In terms of control methods, they range from decentralized methods [8], to admittance based methods [7], passing through flatness and dynamic inversion based methods [9], [10]. The majority of these works present methods to enhance aerial interaction capabilities of aerial vehicle, but only few addressed real tasks that require physical interaction like the previously mentioned NDT (e.g., [11]).

The first contribution of this work is to present one of the first complete aerial robotic solutions with sufficient physical interaction capabilities for generic push-and-slide tasks on curved surfaces. Such achievement goes substantially beyond tasks such as pick&place and pull/push objects, which have been already covered in the literature.

The second main contribution is to demonstrate that such system, endowed with an EC sensor, can successfully inspect a metallic pipe and localize position and orientation of a weld on it. The experiments show that the proposed aerial manipulator is able, similarly to a human operator, to autonomously scan the pipe surface sliding the sensor over it, ensuring the contact and its perpendicularity with respect to (w.r.t.) the surface. The acquired data from the EC sensor are streamed real-time and post-processed in order to detect and exactly locate a weld on the metallic pipe.

The success of the automatic inspection task stems from a wise conception of an aerial manipulator and to the design and integration of methods for the EC sensing, motion planning and control of the robot. In our system, the aerial manipulator is composed by a multidirectional-thrust vehicle endowed with a lightweight arm ending with the EC sensor. The system has been designed in order to have a certain redundancy w.r.t. the task, to grant the system a greater dexterity. Furthermore, the choice to use a multidirectional-thrust vehicle, rather than an unidirectional one, grants a true redundancy. In fact, thanks to its fully actuation, the attitude of the vehicle is not linked to the position (like for underactuated aerial vehicles) and can be independently assigned and controlled according to the task. Furthermore, such platform significantly improves the robustness of the system w.r.t. external disturbances and uncertainties.

A raster scan path is executed to inspect the pipe. This requires the application of a motion planner to generate a robot trajectory respecting the task, system dynamic and input constraints. A simple but effective controller was designed to follow the planned trajectory with sufficiently small errors, preserving the contact with the pipe surface, despite the lack of force feedbacks, the presence of uncertainties (like frictions) and flexibilities of the structure.

The focus of this work stands on the design and control of the aerial manipulator for push-and-slide task for pipe inspection, and on the integration of the robotic system with the sensing one. Therefore, the experimental validation is conducted indoor using a Motion Capture system (MoCap) to retrieve the state of the robot. Nevertheless, we tested the system with degraded MoCap measurements, to emulate the effect of a less accurate localization system. The integration with state-of-the-art pose estimation methods based on on-board sensors is left as future work.

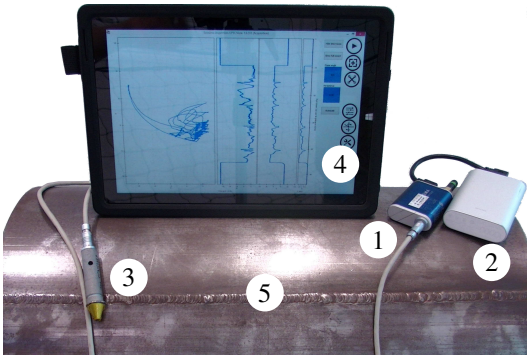

Fig. 2: Measurement setup: The eddy current controller *Sensima UPec* (1), powered by battery (2), and the pen-probe (3) are installed on the aerial robot. The measurements are sent through bluetooth or wifi connection to a PC (4) and are processed by the software *UPecView*. We removed the usual coating/paint that protects and insulates the pipe in order to make the weld visible. However, we remark that the weld is not usually detectable by vision (see Sec. I).

In section II we firstly describe the pipe inspection task. The proposed aerial manipulator and the corresponding design choices are presented in Sec. III. The motion planning and control methods for the execution of the task are described in Sec. IV and Sec. V, respectively. The real inspection and corresponding results are presented in Sec. VII. Final discussions follow in Sec. VIII.

II. PIPE INSPECTION TASK

The detection and localization of a weld on a low carbon steel pipe is the prerequisite to enable successive inspections aimed to verify the element integrity. In this context, an absolute EC probe is used, according to the regulations to detect and localize the weld [12].

In particular, the instrument used for the inspection is a *Sensima UPec* kit, visible in Fig. 2. The output of the sensor is a time varying signal $w(t) \in \mathbb{C}$, the field of complex numbers, related to the properties of the material in contact with the sensor. A change of w represents a change of the material properties. The shape of its trajectory in $\mathbb{C}$ allows to eventually recognize features like a crack, the variation of the metal alloy composition, etc. For a more detailed and exhaustive explanation we refer the interested reader to [1]. An example of signal evolution is depicted in Fig. 6, where the signal path relative to contact-free flight (lift-off) and weld detection are highlighted.

In particular, from w, it is possible to retrieve the magnitude of the signal directly linked to the *lift-off* and the *weld*, denoted by w_l and w_w, respectively. The first is related to the distance from the surface, while the second to the presence or not of a weld. The acquisition software integrates the possibility to extract the amplitude of the signals toward the related trajectories. Such operation takes the advantage of Principal Component Analysis (PCA) and basis transformation, like in [13]. A preliminary calibration

is usually conducted to define the acceptance thresholds for w_l and w_w, denoted by $\bar{w}_l$ and $\bar{w}_w$, respectively. The probe is considered

- in contact with the inspected surface if $w_l < \bar{w}_l$;
- on the weld if both $w_l < \bar{w}_l$ and $w_w > \bar{w}_w$.

Finally, a pipe inspection is conducted performing a *raster scan* (or any other types of scans) with the probe on the surface to localize the weld. Some important manipulation constraints apply to ensure a satisfactory quality of the measurements. In fact, the probe tilt and lift-off w.r.t. the inspected surface shall be minimized during the scan process in order to reduce any spurious effect not related to material change or defects. According to the probe model used in this activity, the sensor should be maintained 1) mostly perpendicular to the surface, with a maximum deviation of around 10°, and 2) with the sensing tip as close as possible to contact, with an air gap always less than 1 [mm]. Those are two important constraints that have to be considered at the motion planning and control levels.

III. AERIAL MANIPULATOR

The inspection task requires the robot to be able to control the full pose of the end-effector, i.e., both position and orientation. Therefore, the robot must have at least 6 Degrees of Freedoms (DoFs). This directly exclude the use of unidirectional-thrust vehicles equipped with a rigid tool ending with the sensor. They are at best able to control only the position of the end-effector and the yaw [5]. One could endow the aerial vehicle with an articulated arm with at least 2 DoFs. However, if the vehicle and the arm are controlled independently, as it has been frequently proposed in previous works, like in [6], the underactuated vehicle cannot instantaneously compensate interaction forces with the arm and the environment. A model-based whole body approach should be used instead, like the ones in [9], [14]. Nevertheless, this is a challenging control problem in real world, and existing techniques lack of robustness w.r.t. disturbances and unknown model parameters.

A recent successful solution for aerial physical interaction is the use of multidirectional-thrust aerial vehicles, like the ones proposed in [15], [16], that are fully actuated in the working region. Such capability allows the aerial platform to exert a six-dimensional wrench in a decoupled fashion [17], permitting to independently control the position and orientation of the robot, and to balance external forces – induced, e.g., by the contact with the environment or by additional loads – almost instantaneously and without the need of reorienting the body, as instead needed by unidirectional-thrust vehicles. In our previous work [7], we showed that a multidirectional-thrust vehicle can successfully interact with the environment by the means of a rigid tool. However, the input limits restrict the admissible orientation of the platform, and in turn of the end-effector. Considering the task described in Sec. II, this limits the area that can be inspected by a multidirectional-thrust vehicle with a rigid tool.

To enlarge the feasible scanning area to the full external surface of a pipe, in this work, we propose the use of multidirectional-thrust aerial vehicle endowed with a planar 2-DoFs lightweight arm ending with a compliant support for the sensor. An image of the robotic system is shown in Fig. 1, and each sub-system is described in the following.

The overall system is characterized by 8 DoFs, that makes it redundant w.r.t. the inspection task. In addition to enlarging the workspace, the 2-DoFs arm and the following redundancy can be also exploited during motion planning to choose the best configuration in terms of input feasibility, manipulability and energy efficiency, and to avoid possible surrounding obstacles (e.g., see [18]).

A. Multidirectional-thrust Aerial Vehicle: the OTHex

The *Open Tilted Hexarotor* (OTHex) is a custom-made aerial robot developed at LAAS-CNRS with the purpose of accomplishing aerial physical interaction tasks. The OTHex is composed by 6 coplanar propellers with a tilted arrangement which enables the multidirectional-thrust property and hence the local full actuation of its dynamics. Another interesting feature of this robot is represented by a frontal aperture within the structure frame, which allows the arm pass through without touching the spinning propellers.

The OTHex was conceived and built in our previous work [19], where it was used with a 1-DoF passive gripper to manipulate long objects like beams. Given the remarkable physical interaction capabilities exhibited in real experiments and demonstrations, such aerial robot was chosen for this inspection task, with some shrewdness. Firstly, the simple manipulation tool was substituted with a lightweight 2-DoF arm, improving the dexterousness required by the sought complex inspection task. Secondly, the frontal aperture is now also used to increase the workspace of the arm, also allowing for frontal and upward operations.

To describe the state of the OTHex, and then of the whole robotic system, we first define a world frame $\mathscr{F}_W = \{O_W, \boldsymbol{x}_W, \boldsymbol{y}_W, \boldsymbol{z}_W\}$, with arbitrarily placed origin O_W, and unit axes $(\boldsymbol{x}_W, \boldsymbol{y}_W, \boldsymbol{z}_W)$ such that $\boldsymbol{z}_W$ points in the opposite direction of the gravity vector. An additional frame $\mathscr{F}_R = \{O_R, \boldsymbol{x}_R, \boldsymbol{y}_R, \boldsymbol{z}_R\}$ is rigidly attached to the OTHex in its Center of Mass (CoM). The position and orientation of the aerial vehicle are defined by the vector $\boldsymbol{p}_R \in \mathbb{R}^3$ and the rotation matrix $\boldsymbol{R}_R \in SO(3)$, respectively. The linear and angular velocities are defined by the vectors $\boldsymbol{v}_R = d\boldsymbol{p}_R/dt$ and $\boldsymbol{\omega}_R \in \mathbb{R}^3$ that is the angular velocity of $\mathscr{F}_R$ w.r.t. $\mathscr{F}_W$ and expressed in $\mathscr{F}_R$.

In the working conditions, we can assume the platform fully actuated, namely capable to independently generate any force $\boldsymbol{f}_R \in \mathbb{R}^3$ and torque $\boldsymbol{\tau}_R \in \mathbb{R}^3$, both expressed in $\mathscr{F}_R$.

B. Articulated Arm and End-effector

The 2-DoFs serial manipulator presents a tensegrity-based structure with the use of prestressed carbon fiber bars connected through 3D printed ABS parts. A similar concept was successfully used for aerial manipulation in [20]. The design choices of an aerial manipulator are always driven by the usual requirements: mass, rigidity, inertia, workspace, compactness, and admissible payload. Here, the sought task

OTHex		2-DoFs arm		Sensor+holder	
mass [kg]	1.6	mass [kg]	0.45	mass [kg]	0.2
diameter [m]	1.2	length link 1 [m]	0.29	length [cm]	13
height [m]	0.3	length link 2 [m]	0.25		

TABLE I: Physical parameters of the aerial manipulator.

leads to the minimization of the mass and inertia of the structure at the expense of the admissible payload, which consists only of the sensor and its support. The tensegrity-based structure helps minimizing the mass while ensuring good torsional and flexural strength. To reduce the inertia effects, the two Dynamixel servomotors MX-64T and MX-28T are fixed to the base of the manipulator as close as possible to the CoM of the aerial platform. The actuation of the second joint is ensured by the mean of a synchronous belt. To limit the risk of collisions, the workspace offers a safety margin between the propellers and the pipe. The design of the arm also enables the manipulator to fold onto itself during the free-flight phase to avoid collisions.

To describe the arm configuration, we rigidly attach to each link a frame $\mathscr{F}_{Ji} = \{O_{Ji}, \boldsymbol{x}_{Ji}, \boldsymbol{y}_{Ji}, \boldsymbol{z}_{Ji}\}$ with $i = 1,2$, following the Denavit-Hartenberg convention. In particular, $\boldsymbol{z}_{Ji}$ is the axis of actuation of the i-th joint and $q_{Ji} \in \mathbb{R}$ denotes the rotation angle about $\boldsymbol{z}_{Ji}$. The configuration of the arm is then given by the vector $\boldsymbol{q}_A = [q_{J1}\ q_{J2}]^\top \in \mathbb{R}^2$, and $\boldsymbol{v}_A = \dot{\boldsymbol{q}}_A \in \mathbb{R}^2$ denotes its velocity.

Each joint is not directly driven by a motor, thus the relation between joint and motor velocities, $\boldsymbol{v}_M = [v_{M1}\ v_{M2}]^\top \in \mathbb{R}^2$, is given by $\boldsymbol{v}_A = \boldsymbol{J}_{AM}\boldsymbol{v}_M$ where $\boldsymbol{J}_{AM} \in \mathbb{R}^{2\times 2}$ is the relative invertible Jacobian matrix. We assume that each motor applies a generalized torque $\tau_{Mi} \in \mathbb{R}$ about the joint axis $\boldsymbol{z}_{Ji}$, for $i = 1,2$. The motor are controlled in velocity, so τ_{Mi} cannot be controlled, but it is computed by a low-level controller based on the actual and desired velocity, $v^\star_{Mi}$.

In order to ensure a continuous contact between the sensor and the pipe during the measurement and despite its tolerance in position, the end-effector needs additional compliance. Hence, the sensor is embedded into a 3D printed custom slider made of nylon-based plastic, with an internal compression spring (see Fig. 1 on the right). To describe the pose of the end-effector, we rigidly attach a frame $\mathscr{F}_E = \{O_E, \boldsymbol{x}_E, \boldsymbol{y}_E, \boldsymbol{z}_E\}$ to tip of the sensor. With $\boldsymbol{p}_E \in \mathbb{R}^3$ and ${}^W\boldsymbol{R}_E \in SO(3)$ we denote the position and orientation of $\mathscr{F}_E$ w.r.t. $\mathscr{F}_W$, respectively. The main physical parameters of the whole robotic system are reported in Tab. I.

C. Dynamic Model

We denote by $\boldsymbol{q} = (\boldsymbol{p}_R, \boldsymbol{R}_R, \boldsymbol{q}_A)$ and $\boldsymbol{v} = [\boldsymbol{v}_R^\top\ \boldsymbol{\omega}_R^\top\ \boldsymbol{v}_A^\top]^\top$ the configuration and the corresponding velocities of the aerial manipulator. Its dynamics can be formulated using the Lagrange method in the following form:

$$\boldsymbol{M}(\boldsymbol{q})\dot{\boldsymbol{v}} = \boldsymbol{c}(\boldsymbol{q},\boldsymbol{v}) + \boldsymbol{g}(\boldsymbol{q}) + \boldsymbol{G}(\boldsymbol{q})\boldsymbol{u}, \tag{1}$$

where $\boldsymbol{M}(\boldsymbol{q}) \in \mathbb{R}^{(6+2)\times(6+2)}$ is the positive-definite inertia matrix, $\boldsymbol{c}(\boldsymbol{q},\boldsymbol{v}) \in \mathbb{R}^{(6+2)}$ is the vector collecting the centrifugal and Coriolis forces, $\boldsymbol{g}(\boldsymbol{q}) \in \mathbb{R}^{(6+2)}$ represents the gravitational term, $\boldsymbol{G}(\boldsymbol{q}) \in \mathbb{R}^{(6+2)\times(6+2)}$ is the input matrix, and $\boldsymbol{u} = [\boldsymbol{f}_R^\top\ \boldsymbol{\tau}_R^\top\ \tau_{M1}\ \tau_{M2}]^\top \in \mathbb{R}^{(6+2)}$ is the vector containing all the inputs of the aerial manipulator. A more detailed derivation can be found in [10].

IV. MOTION PLANNING METHOD

To properly identify and map a weld on the surface of the pipe, one solution is to perform a *raster scan* over the surface of the pipe. During the scan, the inspection method requires the tip of the sensor always in contact with the surface and perpendicular to it. Since the motion of the robot is determined from the task, a task-constrained motion planner is required. At the motion planning level, it is also very important to take into account the dynamics of the aerial manipulator, as well as its kinematics and input limits. For these reasons, we use our previously presented *Control-Aware Motion Planner* [18], a kinodynamic task-constrained motion planner that has been customized for fully-actuated aerial manipulators. It is based on a tight combination of motion planning algorithms and control methods. In particular, a Rapidly-Exploring Random Trees (RRT) algorithm is combined with a second-order inverse kinematics controller that serves as a local planner. This paradigm allows to sample states directly in the task space, extending the exploration tree by simulating the closed-loop system, until a leaf reaches the desired goal. The planner provides the end-effector desired trajectory, $(\boldsymbol{p}_E^d(t), \boldsymbol{R}_E^d(t))$ and the nominal trajectory of each DoF of the aerial manipulator, $(\boldsymbol{p}_R^n(t), \boldsymbol{R}_R^n(t), \boldsymbol{q}_A^n(t))$, respecting the task-constraints, dynamic constraints, and the input limits of the system. For the details, we refer the interested reader to [18]. In the present work, the planner has been extended with a via-point feature to implement the desired raster scan path. The Control-Aware Motion Planner is implemented in C++, using and customizing the open-source ROS package *MoveIt!*[2] and the *OMPL* library[3].

V. CONTROL METHOD

The sought task involves the control of both the pose of the end-effector and the interaction force in order to keep the contact between the end-effector and the surface to be inspected. Simultaneous motion and force control is a well studied problem in the state of the art of classical grounded manipulator and several established methods have been proposed. Some of the most popular are: PD with gravity compensation [21], parallel control [22] for which a position and force controllers work together, impedance control [23] that reshapes the dynamic properties of the system making it compliant with the environment, and hybrid position/force control [24] to precisely control the force and the position along the interaction axes and the perpendicular ones, respectively. For a more detailed and exhaustive presentation of the previously mentioned control strategies we refer to [25] and the citations therein. However, those well known control techniques for standard manipulators cannot be directly applied to aerial manipulators. Indeed most of them rely on the dynamic inversion and on a closed loop

[2] http://moveit.ros.org/
[3] http://ompl.kavrakilab.org/

force action. The first requires an accurate knowledge of the dynamic model and torque controlled motors for the joints of the arm. The two requirements are commonly not fulfilled on aerial manipulators, and in particular in our case. Indeed, the limited payload of the aerial vehicle allows the use of only very lightweight arm (like ours presented in Sec. III-B) actuated by servo motors, at best controlled in velocity. Furthermore, they are characterized by a low stiffness that implies deformations that cannot be easily identified and considered in the dynamic model. Therefore, methods that are based on the dynamic inversion are not feasible for the system in exam. Furthermore, also adding a force sensor at the end-effector might violate the payload constraint. The estimation of the interaction force at the end-effector by methods based on the knowledge of the dynamics and of the inputs is not possible neither. As already said the dynamic parameters of the system are in general not well known, and the torque provided by the motors of the joint is not accessible. Thus, a force feedback to precisely control the interaction is not available and a state-only based controller has to be employed. In this cases the common approach is to foresee a compliance behavior of the end-effector and to plan its trajectory slightly "inside" the surface of interest, as for impedance/compliance control [25]. Thanks to the compliance, the position error will make the system slightly push on the surface preserving the sought contact.

The presented aerial manipulator has three sources of compliance: 1) the PD-based pose control of the aerial vehicle (will be explained in the following), 2) the natural flexibilities of the arm, and 3) the spring in the sensor support. One could only use the first two, rigidly attaching the sensor to the second link of the arm, but most of the interaction force will be absorbed by the arm structure that might subsequently break. For this reason we added a third lightweight mechanical compliance that can absorb most of the interaction force, without stressing the rest too much.

Given the redundancy of the system, the pose control of the end-effector could be done with a standard *Inverse Kinematics Control*, like in [6]. However, we experimentally noticed that, due to the flexibilities of the arm, the vibrations of the end-effector were amplified by the feedback control action, even with very small gains, not guaranteeing the required precision. To use such control approach, the robot should be endowed with a more rigid and so more expensive and heavy arm.

A possible simple solution is to use a joint space control approach in which each actuated DoF independently tracks the nominal joint trajectory provided by the planner. In ideal conditions, namely if the nominal and real kinematics models are the same, a zero tracking error of the nominal joint trajectories would imply a zero tracking error of the end-effector trajectory. However, in real conditions this is never the case due to errors in the servo motors, unmodeled frictions, calibration errors, uncertainties in the kinematic parameters, joints and structural elasticities, and so on. A feedback action w.r.t. the end-effector pose is always needed. We then decided to delegate the feedback action to the OTHex. Since it is fully actuated it can directly control the 6 DoFs of the end-effector. The arm is instead directly controlled in joint space with the following control law:

$$\boldsymbol{v}_M^\star = \boldsymbol{v}_M^n + \boldsymbol{K}_M^P \boldsymbol{e}_M, \tag{2}$$

where $\boldsymbol{e}_M = \boldsymbol{q}_M^n - \boldsymbol{q}_M$, $\boldsymbol{K}_M^P \in \mathbb{R}^{2\times 2}$ is a positive definite matrix. $\boldsymbol{q}_M^n$ and $\boldsymbol{v}_M^n$ are computed from the nominal joints angles and velocities, $(\boldsymbol{q}_A^n, \boldsymbol{v}_A^n)$, by inverse kinematics.

Splitting the task into position and orientation of the end-effector, we experimentally noticed that for the sought task, the arm elasticities and the kinematics errors mainly reflect on the position error of the end-effector. In fact, when we tried the simple joint space controller the attitude error was always below the 10° required by task, while the position error was too much outside task requirement. Therefore, we decided to perform also the attitude control of the vehicle directly in the joint space using the nominal trajectory:

$$\boldsymbol{\tau}_R = \boldsymbol{g}_2(\boldsymbol{q}) + M_{22}\dot{\boldsymbol{\omega}}_R^n + \boldsymbol{K}_R^D \dot{\boldsymbol{e}}_R + \boldsymbol{K}_R^P \boldsymbol{e}_R + \boldsymbol{K}_R^I \int \boldsymbol{e}_R d\boldsymbol{\tau}, \tag{3}$$

where $\boldsymbol{g}_2(\boldsymbol{q}) = \boldsymbol{\Delta_2} \boldsymbol{g}(\boldsymbol{q})$, $M_{22} = \boldsymbol{\Delta_2} \boldsymbol{M}(\boldsymbol{q}) \boldsymbol{\Delta_2}^\top$ in which[4] $\boldsymbol{\Delta_2} = [\boldsymbol{0}_3\ \boldsymbol{I}_3\ \boldsymbol{0}_2]$. $\boldsymbol{K}_\star^R \in \mathbb{R}^{3\times 3}$ are positive definite matrices. Then, $\boldsymbol{e}_R = \frac{1}{2}[\boldsymbol{R}_R^\top \boldsymbol{R}_R^n - \boldsymbol{R}_R^{n\top} \boldsymbol{R}_R]_\vee$ in which $[\star]_\vee$ is the inverse of the skew map, $\dot{\boldsymbol{e}}_R = \boldsymbol{\omega}_R^n - \boldsymbol{\omega}_R$.

Regarding the position control of the vehicle, it has to include the feedback from the end-effector position in order to compensate for all the errors due to the many non-perfectly known kinematic and dynamic parameters. However, the design of such control action has to be done carefully due to the presence of elasticities. In view of this, we naturally took inspiration from the state-of-the-art on control of manipulators with elastic joints [26]. Comparing our situation with a manipulator with elastic joints, we can consider the OTHex as a 6-dimensional motor and the arm plus the compliant sensor holder as a single elastic joint. Inspired by this analogy, we decided to apply a 'dislocated' PD control law, e.g., a PD with a mixed feedback strategy. In fact, it has been proved that for an 1-DoF manipulator with an elastic joint in the one dimensional case, a feedback action entirely based on the end-effector position and velocity leads to instability, no matter the gain values. On the other hand, a mixed feedback from the link position and motor velocity ensures stability if the gains are properly chosen [26]. The proposed position controller employs such a mixed feedback strategy using the position of the end-effector and the translational velocity of the aerial vehicle in the feedback loop:

$$\boldsymbol{f}_R = \boldsymbol{R}_R^\top (\boldsymbol{g}_1(\boldsymbol{q}) + M_{11}\dot{\boldsymbol{v}}_R^n + \boldsymbol{K}_P^D \dot{\boldsymbol{e}}_R + \boldsymbol{K}_P^P \boldsymbol{e}_E + \boldsymbol{K}_P^I \boldsymbol{\sigma}(\boldsymbol{e}_E)), \tag{4}$$

where $\boldsymbol{g}_1(\boldsymbol{q}) = \boldsymbol{\Delta_1} \boldsymbol{g}(\boldsymbol{q})$, $M_{11} = \boldsymbol{\Delta_1} \boldsymbol{M}(\boldsymbol{q}) \boldsymbol{\Delta_1}^\top$ in which $\boldsymbol{\Delta_1} = [\boldsymbol{I}_3\ \boldsymbol{0}_3\ \boldsymbol{0}_2]$. $\boldsymbol{K}_P^\star \in \mathbb{R}^{3\times 3}$ are positive definite matrices. Then, $\boldsymbol{e}_E = \boldsymbol{p}_E^d - \boldsymbol{p}_E$, $\dot{\boldsymbol{e}}_R = \boldsymbol{v}_R^n - \boldsymbol{v}_R$. Notice that in (3) and (4) we neglected the dynamic couplings and Coriolis terms since a quasi static condition is required for the sought task.

[4] $\boldsymbol{I}_i \in \mathbb{R}^{i\times i}$ is the identity matrix of dimension i.

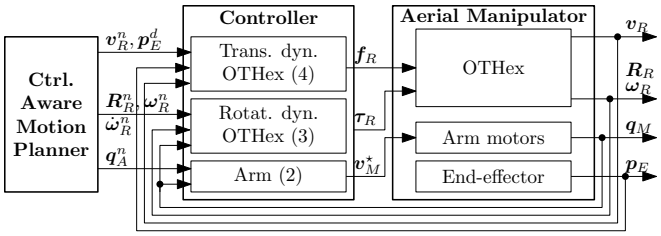

Fig. 3: Schematic representation of the controller.

Finally, the function $\boldsymbol{\sigma}(\boldsymbol{e}_E)$ implements a particular integral action with dead-zone, done in the *interaction frame*, $\mathscr{F}_I = \{O_I, \boldsymbol{x}_I, \boldsymbol{y}_I, \boldsymbol{z}_I\}$. While performing the desired task, namely when the sensor is in contact with the surface we define $\mathscr{F}_I$ such that O_I coincides with O_E and $\boldsymbol{z}_I$ is directed as the normal to the surface at the point O_I. $\boldsymbol{x}_I$ and $\boldsymbol{y}_I$ are arbitrary. Then we denote by $\boldsymbol{R}_I \in SO(3)$ the rotation matrix describing the attitude of $\mathscr{F}_I$ w.r.t. $\mathscr{F}_W$. The integral action $\boldsymbol{\sigma}(\boldsymbol{e}_E)$ is then defined such as

$$\dot{\boldsymbol{\sigma}}(\boldsymbol{e}_E) = \begin{cases} \boldsymbol{R}_I \begin{bmatrix} 1 & 0 & 0 \\ 0 & 1 & 0 \\ 0 & 0 & 0 \end{bmatrix} \boldsymbol{R}_I \boldsymbol{e}_E & \text{if} \quad |\begin{bmatrix} 0 & 0 & 1 \end{bmatrix} \boldsymbol{R}_I \boldsymbol{e}_E| < \varepsilon_I \\ \boldsymbol{e}_E & \text{otherwise} \end{cases}$$

The integral action is needed to bring the error to zero at steady state in case of external disturbances or unknown parameters (similarly in (3)). However, along the direction of interaction $\boldsymbol{z}_I$, the error will never go to zero, since the desired end-effector trajectory is slightly inside the pipe. Then, to avoid an infinite growth of the integral along $\boldsymbol{z}_R$, the latter is stopped when the error along $\boldsymbol{z}_R$ in $\mathscr{F}_I$, i.e., $\begin{bmatrix} 0 & 0 & 1 \end{bmatrix} \boldsymbol{R}_I \boldsymbol{e}_E$, is between a certain positive threshold, $\varepsilon_I \in \mathbb{R}$, that has to be set according to the compliance of the system.

Figure 3 visually describes the controller. Summarizing, a direct measure or an estimation of the following variables is needed: $\boldsymbol{v}_R$, $\boldsymbol{R}_R$, $\boldsymbol{\omega}_R$, $\boldsymbol{q}_M$ (or equivalently $\boldsymbol{q}_A$) and $\boldsymbol{p}_E$.

VI. SOFTWARE ARCHITECTURE

The software developed for the presented aerial manipulator comprises many independent and interconnected components. The resulting software architecture is made of only in house open source software.

At the lowest level, the OTHex runs a custom software on a Mikrokopter brushless controllers (8bit Atmega MCU). The code implements a closed loop, precise propeller velocity controller [27] and communicates via an I2C bus with a Mikrokopter flight controller. The precise control of the spinning velocity is very important for an accurate actuation of the desired wrench. The flight controller acts as a proxy between the brushless motors and the higher software levels. It also exports the raw, analog 6D IMU readings to the higher software levels. Both components run at 1kHz.

The higher software layer is made of a variable number of independent components, including at least:

1) A UAV driver component interfacing with the flight controller through a USB UART link. It sends the desired propeller velocities to the hardware and exports actual measurements, IMU, current consumption etc.

2) A Dynamixel motor driver component interfacing with the 2-DoFs arm. It sends the desired velocity to each motor and reads its actual velocity and position.

3) A UKF based state estimation component, running at 1kHz, that fuses data from IMU, motion capture system or any other source.

4) A motion capture component reading multiple rigid body (namely OTHex and end-effector) position and orientation from an Optitrack system, from 30 [Hz] to 100 [Hz].

Most of those components have been developed in C++ and can run either on-board or on a off-board desktop PC. The actual control components (attitude, position and physical interaction) are currently developed in Matab/Simulink and run on a ground PC at 500 [Hz]. Those components will be soon implemented in C++ too, so that the whole demonstration can run on an embedded computer.

As for most of the robotics software at LAAS-CNRS, software components have been developed using *GenoM3* [28], a code generator and formal software component description language that allows to assemble middleware-independent components in a modular system. Most of this software is available on the *openrobots* repository at `https://git.openrobots.org/projects/telekyb3`

VII. EXPERIMENTAL RESULTS

The experiment presented next is the final result of a well-thought robot conception and of the integration of motion planning and control methods together with sensing technologies. The experiment is aimed to demonstrate the effectiveness of the proposed aerial manipulator system to perform inspection tasks requiring physical contact, reached after a series of numerous simulations and preliminary experimental tests, needed for the design and control tuning.

The goal in the experiment is to identify and localize a weld on a portion of metallic pipe (see Figs. 2 and 1) of length 0.5 [m] and diameter 0.4 [m], using an EC probe. The inspection is performed on a section of the pipe with arc of 40°, by means of a raster scan path composed by 8 corners (passing over the weld 4 times). Giving the set of waypoints as input to the proposed motion planner, we obtain the desired end-effector trajectory and the nominal trajectories of the robot DoFs shown in Figs. 4 and 5, respectively. The contact-inspection trajectory has a duration of 110 [s] and is planned in around 9 [s] on a standard laptop (Intel i5, 3.2 [GHz], 6GB RAM).

The overall experiment is composed of three parts: i) approach of the pipe (arm folded and sensor not in contact), ii) contact-based inspection, and iii) departure from the pipe to finally land. Here, we focus our analysis on the most interesting part ii). For this part of the experiment, Figs. 4, 5 and 6 show the behavior of the robot and the acquired data by the sensor, from right before contact (time 25 [s]) to right after contact (once the inspection is over, time 144 [s]).

From Figs. 4 and 5, one can appreciate the accuracy of the robot to track the desired end-effector trajectory, with sufficiently small tracking error keeping always the contact (confirmed by the value of w_l). This is done despite the presence of many uncertainties, elasticities, frictions and no force

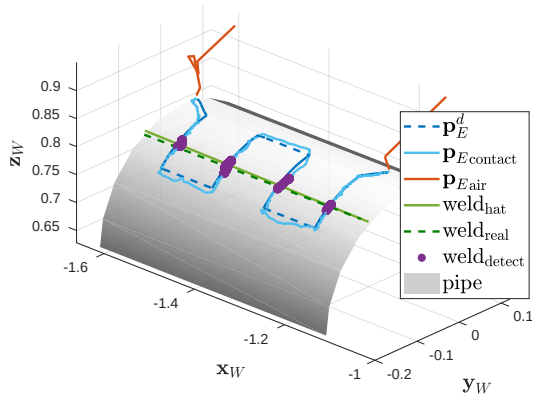

Fig. 4: Representation of the desired and actual trajectories of the end-effector over the pipe. The purple dots highlight the points in which the weld is detected.

feedback. The presence of errors in the kinematic model is confirmed by the non-zero error between the nominal and actual pose of the aerial vehicle. If the kinematic model was known exactly, an almost-zero end-effector pose error would have implied an almost-zero error between the nominal and actual state, and vice versa.

Note that once the robot gets in contact with the surface, the (unknown) interaction force exerts an extra torque on the aerial vehicle, which implies an orientation error. However, this error goes to zero in few seconds as a result of the integral term in (3), which can act effectively and independently from the position control thanks to the full actuation of the OTHex. During the transient, this inaccuracy induces a small error in the end-effector orientation too. The latter is defined by the vector $\boldsymbol{e}_{E\eta} = [e_{E\phi}\ e_{E\theta}\ e_{E\psi}]^\top$ where $e_{E\phi} = \phi_E^d - \phi_E$. Analogously for $e_{E\theta}$ and $e_{E\psi}$. $(\psi_E, \theta_E, \phi_E)$ are the Euler-angles describing the orientation of $\mathscr{F}_E$, following the convention Z-Y-X. The end-effector pose error always respects the task requirements.

Fig. 6 shows the raw signal $w(t)$ coming from the EC sensor. It is interesting to notice its evolution when the probe passes from air to contact and vice-versa, and over the weld. From $w(t)$, applying the mentioned PCA method, we can retrieve the more informative signals w_l and w_w (shown in Fig. 5). The contact phase can be identified looking at when $w_l < \bar{w}_l = 15$. On the other hand, looking at w_w for $w_w > \bar{w}_w = 1.4$ and $w_l < \bar{w}_l$, we can identify when the probe is in contact with the weld. The thresholds $\bar{w}_l$ and $\bar{w}_w$ were identified in a preliminary calibration phase. In all the plots, we highlight the no-contact and contact-with-weld phases with red and purple colors, respectively.

Combining w_w with the measured position of the probe, we retrieved an estimation of the weld position all along the surface, using a simple linear regression technique. The estimated and the real weld positions are shown in Fig. 4 by green solid and dashed lines, respectively.

In view of a future integration with a vision system for outdoor experimentation, we tested the proposed robotic system with degraded MoCap measurements and the presence of wind. Our test shown that reducing the state-update frequency down to 30 [Hz] (comparable to a minimal onboard

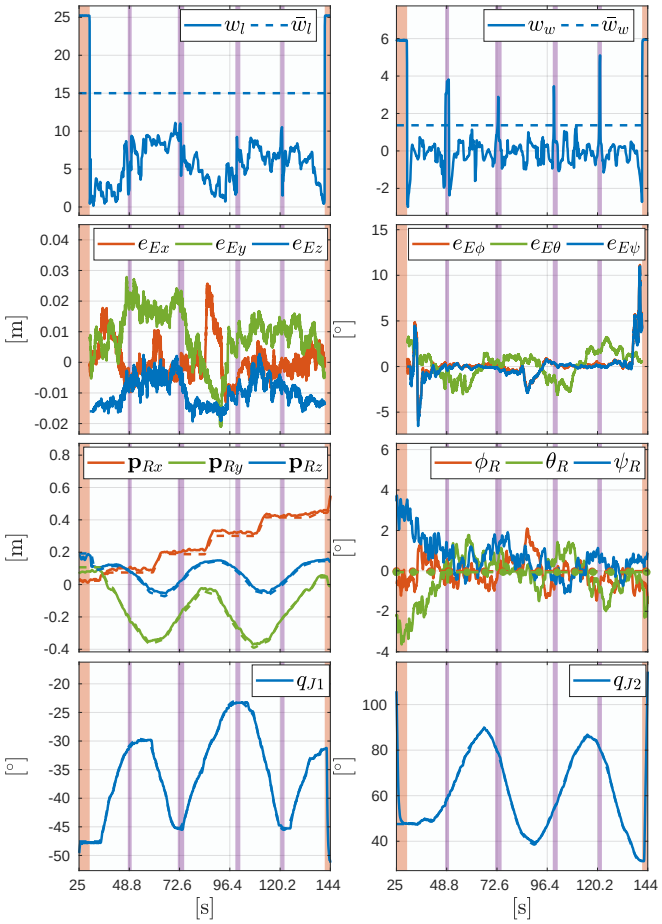

Fig. 5: Evolution of the main variables. The dashed lines in the last four plots represent the nominal trajectories given by the motion planner. The orientation of the aerial vehicle is here represented by the Euler-angles $(\psi_R, \theta_R, \phi_R)$ following the convention Z-Y-X.

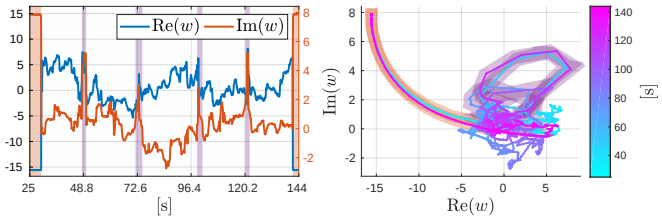

Fig. 6: Acquired raw data w, showing its real and imaginary parts and its evolution in $\mathbb{C}$. On the right image, the color of the line represents the time.

vision system) has no influence in the tracking performance and neither on the quality of the acquired EC data. Similarly, the presence of a fan (both in static and dynamic modality) blowing air on the robot at a speed of around 6 [m/s] has almost no effect on the quality of the results. The relative results are presented in the following. A video of the experiment is attached to the paper.

A. *Additional experiments in degraded conditions*

In view of a future integration with a vision system for outdoor experimentation, we tested the proposed robotic system with degraded MoCap measurements and the presence of wind.

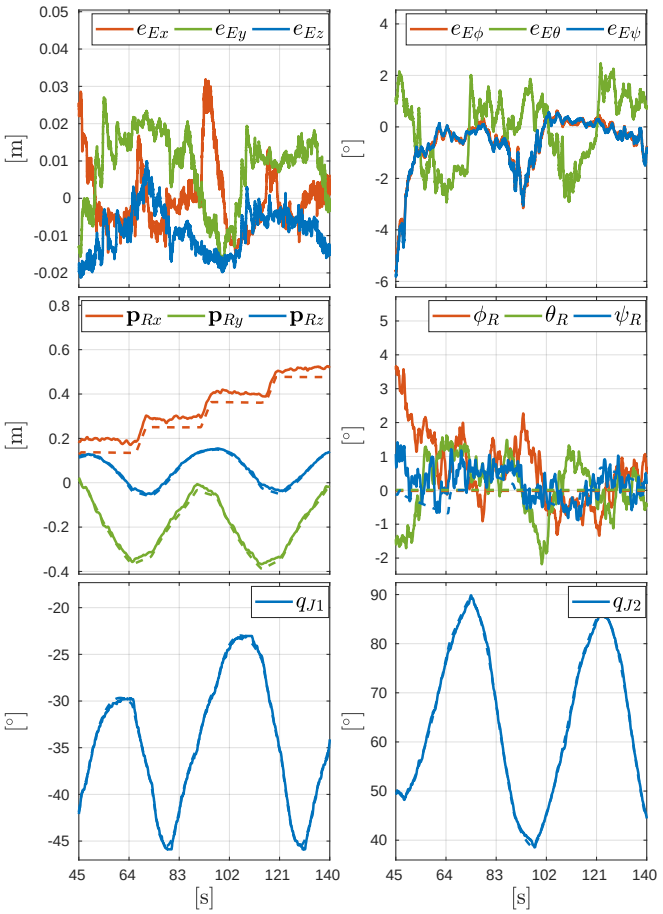

Fig. 7: Main variables when the MoCap frequency is reduced to 30 [Hz]

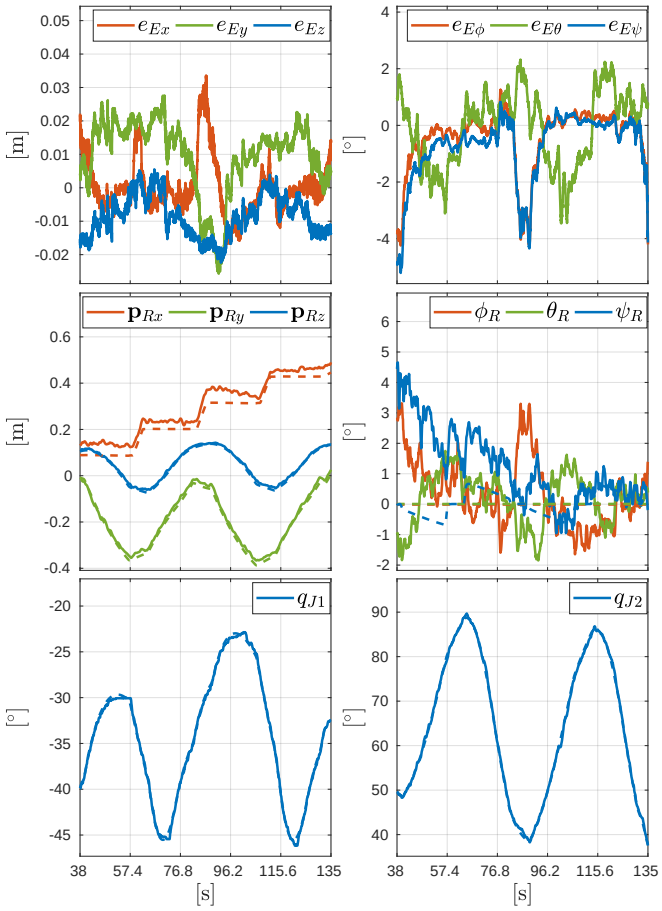

Fig. 8: Main variables when the aerial manipulator subjected by an external force produce by wind.

1) Degraded MoCap measurements: In this section we report the tracking performances of the proposed robotic system when the update rate of the state is reduced. In particular, in Fig. 7 we report the experimental results during the interaction phase, when the MoCap frequency is set to only 30 [Hz]. Comparing those results with the ones obtain with the MoCap running at 100 [Hz] (see Fig. 5) we can conclude that there are not differences.

2) External disturbance: wind: In this experiment a domestic fan blows air toward the aerial manipulator. The air has a speed of around 6 [m/s]. In Fig. 8 we report the corresponding results. Also in this case, comparing the results with the one in absence of wind (see Fig. 5) we can spot any relevant differences. We can conclude that the proposed robotic system is also robust to sufficiently bounded external disturbances.

VIII. CONCLUSIONS

In this work, we considered the challenging physical interaction task of pushing while sliding on curved surfaces with an aerial manupulator, going beyond the simpler pick&place and pull/push tasks. In this case, both the pose of the end-effector and the interaction force have to be precisely controlled. We proposed one of the first aerial manipulator systems capable to perform such task in the context of a real and relevant application: EC inspection of metallic pipes. The successful results further validated the effectiveness of multidirectional-thrust aerial vehicles for physical interaction, in this case also incorporating a lightweight arm. Particular attention was required in the control design to enable steer the end-effector along the desired trajectory while preserving the contact. In fact, well-known hybrid position/force control methods cannot be applied to such aerial manipulator for the lack of model accuracy and force feedback. The presence of elasticities in the arm structure hampers the application of inverse-kinematics-based control methods. To face those problems, we designed a selective and displaced PID-based controller inspired by the control of manipulators with elastic joints. Together with a suitable task-constrained motion planning method, we demonstrated the capability of the robot to perform the task, detecting and mapping the weld accurately.

The robotic system will be employed in the near feature also for the detection of cracks along the weld. Another natural follow-up of this work will be the integration with an on-board localization and sensing system to perform the task outdoor in a real industrial plant.

REFERENCES

[1] J. García-Martn, J. Gómez-Gil, and E. Vázquez-Sánchez, "Non-destructive techniques based on eddy current testing," *Sensors*, vol. 11, no. 3, pp. 2525–2565, 2011.

[2] E. Gasparin, G. Santi, and A. Nussbaumer, "Eddy Current Crack Monitoring System for Structural Health Monitoring (SHM) Applications," *68th International Institute for Welding (IIW) Annual Assembly and International Conference, Helsinki, Finland, June 29-July 3, 2015*, 2015.

[3] J. V. Miro, D. Hunt, N. Ulapane, and M. Behrens, "Towards automatic robotic ndt dense mapping for pipeline integrity inspection," in *Field and Service Robotics*, M. Hutter and R. Siegwart, Eds. Cham: Springer International Publishing, 2018, pp. 319–333.

[4] A. Ollero, G. Heredia, A. Franchi, G. Antonelli, K. Kondak, A. S. Cortes, A. Viguria, J. R. M. de Dios, F. Pierri, J. Cortés, A. Santamaria-Navarro, M. A. T. Soto, R. Balachandran, J. Andrade-Cetto, and A. R. Castano, "The aeroarms project: Aerial robots with advanced manipulation capabilities for inspection and maintenance," *IEEE Robotics Automation Magazine*, 2018.

[5] H.-N. Nguyen, C. Ha, and D. Lee, "Mechanics, control and internal dynamics of quadrotor tool operation," *Automatica*, vol. 61, pp. 289–301, 2015.

[6] F. Ruggiero, M. A. Trujillo, R. Cano, H. Ascorbe, A. Viguria, C. Perz, V. Lippiello, A. Ollero, and B. Siciliano, "A multilayer control for multirotor uavs equipped with a servo robot arm," in *2015 IEEE Int. Conf. on Robotics and Automation*, Seattle, WA, May 2015, pp. 4014–4020.

[7] M. Ryll, G. Muscio, F. Pierri, E. Cataldi, G. Antonelli, F. Caccavale, and A. Franchi, "6D physical interaction with a fully actuated aerial robot," in *2017 IEEE Int. Conf. on Robotics and Automation*, Singapore, May 2017, pp. 5190–5195.

[8] K. Kondak, K. Krieger, A. Albu-Schäffer, M. Schwarzbach, M. Laiacker, I. Maza, A. Rodriguez-Castano, and A. Ollero, "Closed-loop behavior of an autonomous helicopter equipped with a robotic arm for aerial manipulation tasks," *International Journal of Advanced Robotic Systems*, vol. 10, pp. 1–9, 2013.

[9] M. Tognon, B. Yüksel, G. Buondonno, and A. Franchi, "Dynamic decentralized control for protocentric aerial manipulators," in *2017 IEEE Int. Conf. on Robotics and Automation*, Singapore, May 2017, pp. 6375–6380.

[10] M. Ryll, D. Bicego, and A. Franchi, "A truly redundant aerial manipulator exploiting a multi-directional thrust base," in *2018 IFAC Symp. on Robot Control*, Budapest, Hungary, Aug. 2018.

[11] K. Alexis, G. Darivianakis, M. Burri, and R. Siegwart, "Aerial robotic contact-based inspection: planning and control," *Autonomous Robots*, vol. 40, no. 4, pp. 631–655, 2016.

[12] "Non-destructive examination of welds. Eddy current examination of welds by complex plane analysis," BSI - British Standard Institution, CEN - European Committee for standardization, Standard BS EN 1711:2000, May 2000.

[13] I. Jolliffe, *Principal Component Analysis*. Berlin, Heidelberg: Springer Berlin Heidelberg, 2011, pp. 1094–1096.

[14] H. Yang and D. Lee, "Dynamics and control of quadrotor with robotic manipulator," in *Robotics and Automation (ICRA), 2014 IEEE International Conference on*. IEEE, 2014, pp. 5544–5549.

[15] D. Brescianini and R. D'Andrea, "Design, modeling and control of an omni-directional aerial vehicle," in *2016 IEEE Int. Conf. on Robotics and Automation*, Stockholm, Sweden, May 2016, pp. 3261–3266.

[16] S. Park, J. J. Her, J. Kim, and D. Lee, "Design, modeling and control of omni-directional aerial robot," in *2016 IEEE/RSJ Int. Conf. on Intelligent Robots and Systems*, Daejeon, South Korea, 2016, pp. 1570–1575.

[17] M. Ryll, D. Bicego, and A. Franchi, "Modeling and control of FAST-Hex: a fully-actuated by synchronized-tilting hexarotor," in *2016 IEEE/RSJ Int. Conf. on Intelligent Robots and Systems*, Daejeon, South Korea, Oct. 2016, pp. 1689–1694.

[18] M. Tognon, E. Cataldi, H. Tello Chavez, G. Antonelli, J. Cortés, and A. Franchi, "Control-aware motion planning for task-constrained aerial manipulation," *IEEE Robotics and Automation Letters, Special Issue on Aerial Manipulation*, vol. 3, no. 3, pp. 2478–2484, 2018.

[19] N. Staub, D. Bicego, Q. Sablé, V. Arellano-Quintana, S. Mishra, and A. Franchi, "Towards a flying assistant paradigm: the OTHex," in *2018 IEEE Int. Conf. on Robotics and Automation*, Brisbane, Australia, May 2018.

[20] R. Cano, C. Perez, F. Pruaño, A. Ollero, and G. Heredia, "Mechanical design of a 6-dof aerial manipulator for assembling bar structures using uavs," 2014.

[21] S. Chiaverini, B. Siciliano, and L. Villani, "Force/position regulation of compliant robot manipulators," *IEEE Transactions on Automatic Control*, vol. 39, no. 3, pp. 647–652, March 1994.

[22] S. Chiaverini and L. Sciavicco, "The parallel approach to force/position control of robotic manipulators," *IEEE Transactions on Robotics and Automation*, vol. 9, no. 4, pp. 361–373, Aug 1993.

[23] N. Hogan, "Impedance control: An approach to manipulation: Part IIimplementation," *Journal of dynamic systems, measurement, and control*, vol. 107, no. 1, pp. 8–16, 1985.

[24] A. De Luca and C. Manes, "Modeling of robots in contact with a dynamic environment," *IEEE Trans. on Robotics and Automation*, vol. 10, no. 4, pp. 542–548, 1994.

[25] C. C. de Wit, B. Siciliano, and G. Bastin, "Motion and force control," in *Theory of robot control*. Berlin: Springer Verlag, 1996, ch. 4, pp. 141–175.

[26] A. De Luca and W. Book, "Robots with flexible elements," in *Springer Handbook of Robotics, B. Siciliano, O. Khatib*. Berlin: Springer Verlag, 2008, ch. 13, pp. 287–317.

[27] A. Franchi and A. Mallet, "Adaptive closed-loop speed control of BLDC motors with applications to multi-rotor aerial vehicles," in *2017 IEEE Int. Conf. on Robotics and Automation*, Singapore, May 2017.

[28] A. Mallet, C. Pasteur, M. Herrb, S. Lemaignan, and F. Ingrand, "Genom3: Building middleware-independent robotic components," *2010 IEEE International Conference on Robotics and Automation*, pp. 4627–4632, 2010.